analytical chemistry

Article

Sheathless Focusing and Separation of Diverse Nanoparticles in Viscoelastic Solutions with Minimized Shear Thinning

Chao Liu, Baoquan Ding, Chundong Xue, Yu Tian, Guoqing Hu, and Jiashu Sun

Anal. Chem., **Just Accepted Manuscript** • DOI: 10.1021/acs.analchem.6b04564 • Publication Date (Web): 25 Nov 2016

Just Accepted

ACS Publications

Analytical Chemistry is published by the American Chemical Society. 1155 Sixteenth Street N.W., Washington, DC 20036

Sheathless Focusing and Separation of Diverse Nanoparticles in Viscoelastic Solutions with Minimized Shear Thinning

Chao Liu,[†, ‡, //] Baoquan Ding,[//] Chundong Xue,[†, ‡] Yu Tian,[¶] Guoqing Hu,*[†, ‡] and Jiashu Sun*[//]

[†]State Key Laboratory of Nonlinear Mechanics, Beijing Key Laboratory of Engineered Construction and Mechanobiology, Institute of Mechanics, Chinese Academy of Sciences, Beijing 100190, China. Fax: +86-10-82543977; Email: guoqing.hu@imech.ac.cn

[‡]School of Engineering Science, University of Chinese Academy of Sciences, Beijing 100049, China.

[//]CAS Key Laboratory for Biological Effects of Nanomaterials and Nanosafety, CAS Center for Excellence in Nanoscience, National Center for NanoScience and Technology, Beijing100190, China. Fax: +86-10-82545631; Email: sunjs@nanoctr.cn.

[¶]State Key Laboratory of Tribology, Tsinghua University, Beijing 100084, China.

ABSTRACT: Viscoelastic microfluidics becomes an efficient and label-free hydrodynamic technology to enrich and separate micrometer-scale particles, including blood cells, circulating tumor cells, and bacteria. However, the manipulation of nanoscale particles by viscoelastic microfluidics remains a major challenge because the viscoelastic force acting on the smaller particle decreases dramatically. In contrast to the commonly used polymer solutions of high molecular weight, herein we utilize the aqueous solutions of polyethylene oxide (PEO) of low molecular weight with minimized shear thinning but sufficient elastic force for high-quality focusing and separation of various nanoparticles. The focusing efficiencies of 100 nm polystyrene (PS) nanoparticles and λ-DNA molecules are 84 % and 85 %, respectively, in a double spiral microchannel without the aid of sheath flows. Furthermore, we demonstrate the size-based viscoelastic separation of two sets of binary mixtures, 100/2000 nm PS particles and λ-DNA molecules/blood platelets, all achieving separation efficiencies above 95 % in the same device. Our proposal technique would be a promising approach for enrichment/separation of the nanoparticles encountered in applications of analytical chemistry and nanotechnology.

Precise manipulation of synthetic and biologic nanoparticles is an essential process in many areas of analytical chemistry, biology, and nanotechnology.[1-4] The implement of synthetic nanoparticles and the detection of the biological nanoparticles often require the enrichment and separation of these nanoscale objects by size first.[5-8] Recently, viscoelastic microfluidics has emerged as an efficient and label-free hydrodynamic technology to enrich and separate micrometer-scale particles, including blood cells, circulating tumor cells, and bacteria. The operating principle of this method is based on the deterministic lateral migration of particles induced by the viscoelastic forces in the shear flow of a polymer solution.[9-11] The viscoelasticity is typically characterized using the Weissenberg number Wi ($Wi = \lambda\dot{\gamma}$, where λ is the relaxation time of a polymer solution and $\dot{\gamma}$ the shear rate). The lateral migration velocity $V \propto \kappa^2 Wi$ where κ is the blockage ratio of the particle ($\kappa = a/D_h$, here a is the particle diameter and D_h the channel cross-sectional dimension). A number of studies have demonstrated the focusing and separation of a variety of microparticles and cells by size in viscoelastic solutions based on diverse principles: using sheath flow to initially align all particles and subsequently utilizing the dependency of lateral migration speed on particle size,[12] utilizing hydrodynamic interactions between particles and channel structures, such as elasto-enhanced pinched flow fractionation,[13,14] or introducing Dean flow to compete with elastic lift forces using curved channel geometry.[15,16]

Despite the efforts of manipulation of microparticles in viscoelastic microfluidics, few studies have attempted to investigate the focusing and separation of nanoparticles by viscoelastic forces. Very recently, the focusing of particles with a down to 200 nm (κ = 0.04) in square or circular channels with D_h = 5 μm has been demonstrated in aqueous solutions of PEO with high M_w = 2-4×10^6 g/mol. However, the focusing of particles smaller than 200 nm has not been successfully achieved, due to the dramatically decreased viscoelastic force F_e acting on the smaller particles ($F_e \propto a^3$).[17,18] Moreover, we have shown that the shear thinning effect associated with high M_w polymer solutions may undermine the focusing performance of microparticles,[19] which should be also taken into account when handling the nanoparticles. To effectively focus and sort the nanoparticles, it is critical to balance the requirement of increasing the viscoelastic lift and minimizing the shear thinning effect from the engineered viscoelastic medium, which has not been thoroughly studied yet.

In this work, we aim at addressing the challenges related to nanoparticle manipulating in viscoelastic microfluidics as follows: 1) how to realize the manipulation of nanoparticles within a relatively large-dimensional and easily-fabricated microfluidic platform, and 2) how to choose the carrier medium to improve the focusing performance. In response to these challenges, we carefully characterize the dependence of focusing quality of nanoparticles on molecular weight and concentration of polymer, flow speed, and particle size to find optimal parameters inside a double spiral microchannel

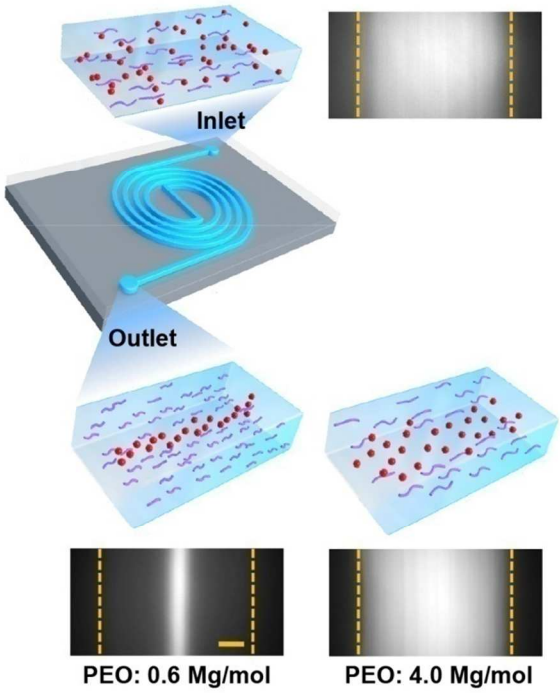

Figure 1. Schematics of the viscoelastic focusing of nanoparticles using PEO solutions of M_w = 0.6×10^6 g/mol in a double spiral microchannel (not to scale). Stacked fluorescent images (top view) show that initially dispersed 100 nm particles are tightly focused at the outlet using a PEO solution of M_w = 0.6×10^6 g/mol and c = 0.6 wt %. In contrast, the 100 nm particles remain unfocused in a PEO solution of M_w = 4.0×10^6 g/mol and c = 0.25 wt %. The scale bar for the fluorescent images corresponds to 5 μm.

(Figure 1). The applicable particle size and focusing quality are found to be the smallest and the highest for PEO solutions with low M_w of 0.6×10^6 g/mol that have weak shear thinning. Using those optimized experimental parameters, we might, for the first time, realize the sheathless and passive manipulation of nanoparticles with dimension less than 100 nm in a simple microfluidic devices.

DESIGN PRINCIPLES AND EXPERIMENTS

Device Design and Fabrication. The double spiral microchannel consists of 5 loops for each spiral, resulting in a total length exceeding 60 mm (Figure S-1 in the SI†). The microchannel, with a width (W) of 30 μm and height (H) of 4 μm, has an aspect ratio (AR = W/H) of 7.5. This high-AR design reduces the proportion of particles unfavorably migrating toward the channel corners, where the elastic lift forces are wall-directed (as shown in Figure 2a-b). Inertial lift is negligible as $Wi/Re > 400$ (here Reynolds number Re characterizes the fluid inertia), which is validated by the absence of particle focusing in deionized water at a wide range of flow speeds up to 87 mm/s, at which the corresponding Re is only 0.61 (Figure S-2 in the SI†). We thus compute the particle trajectories solely dominated by elastic lift forces (see more details in the ESI†) and find that the proportion of particles reaching the channel corners decreases with increasing AR: only 4.5% particles reach the channel corners for AR = 8 compared with 23% for AR = 1 (Figure 2c). The rotation direction of the spiral microchannel changes at a

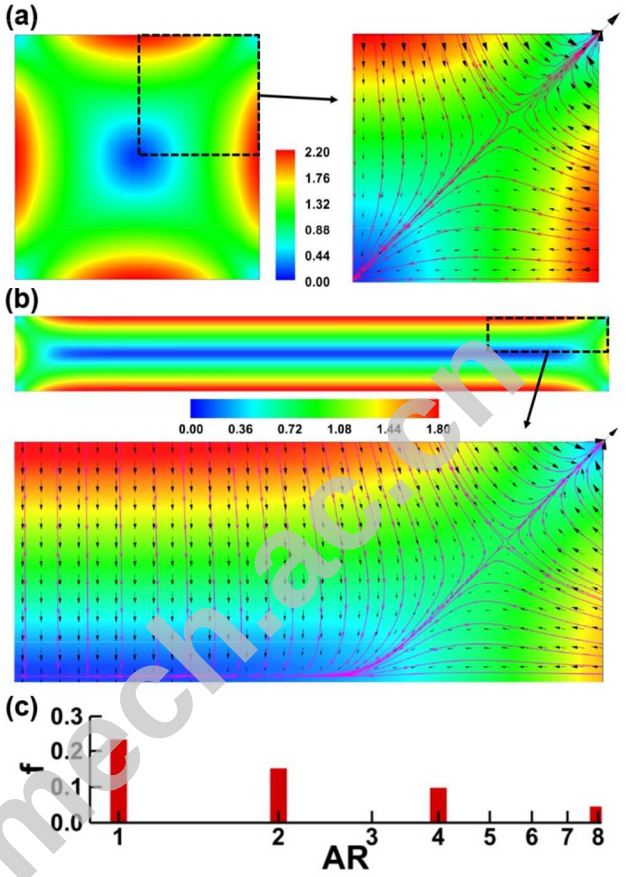

Figure 2. (a-b) The distributions of the square of the normalized shear rate $\dot{\gamma}^2$ and the vectors of the elastic lift forces $\mathbf{F}_e \sim \nabla\dot{\gamma}^2$ and the particle trajectories in microchannels with AR = 1 (a) and 8 (b), respectively. The shear rate is normalized by half channel height and the maximum channel velocity. (c) The fractions f of cross-section areas where particles initially start are finally focused in the channel corners for AR = 1, 2, 4, and 8.

straight junction, avoiding focusing degradation due to the elastic instability onset in a highly curved channel.[20] This straight junction design also minimizes the effect of secondary flow on the particle focusing. The maximum Dean number De obtained at the innermost loops is only 1.3×10^{-3}, suggesting very weak secondary flows (Figure S-3 in the SI†). The microchannel is made of poly(dimethylsiloxane) (PDMS) bonded by a cover class (160 μm thick) using the standard fabrication technique.[21] The detailed procedures have been discussed in our previous papers.[22,23]

Sample Preparation. For PS microspheres experiments, the PEO solutions were prepared by dissolving PEO (M_w = 0.3, 0.6, 1, 2, 4, and 8×10^6 g/mol, Sigma-Aldrich, USA) powder in deionized water (Milli-Q, USA). For the focusing of DNA molecules and DNA origami structures, the PEO solutions were prepared using 1× Tris-EDTA buffer solution. as the solvent, which was prepared by the dilution of a 100× Tris-EDTA buffer solution (1M Tris-HCl, 10 mM EDTA, Cat# T9285, Sigma-Aldrich, USA). For the separation of λ-DNA and platelets, the PEO solutions were prepared using 1× PBS solution (Sigma-Aldrich, USA) as the solvent. The dissolution of PEO powder was accelerated by 1 hour of gently stirring (less than 30 RPM, high M_w

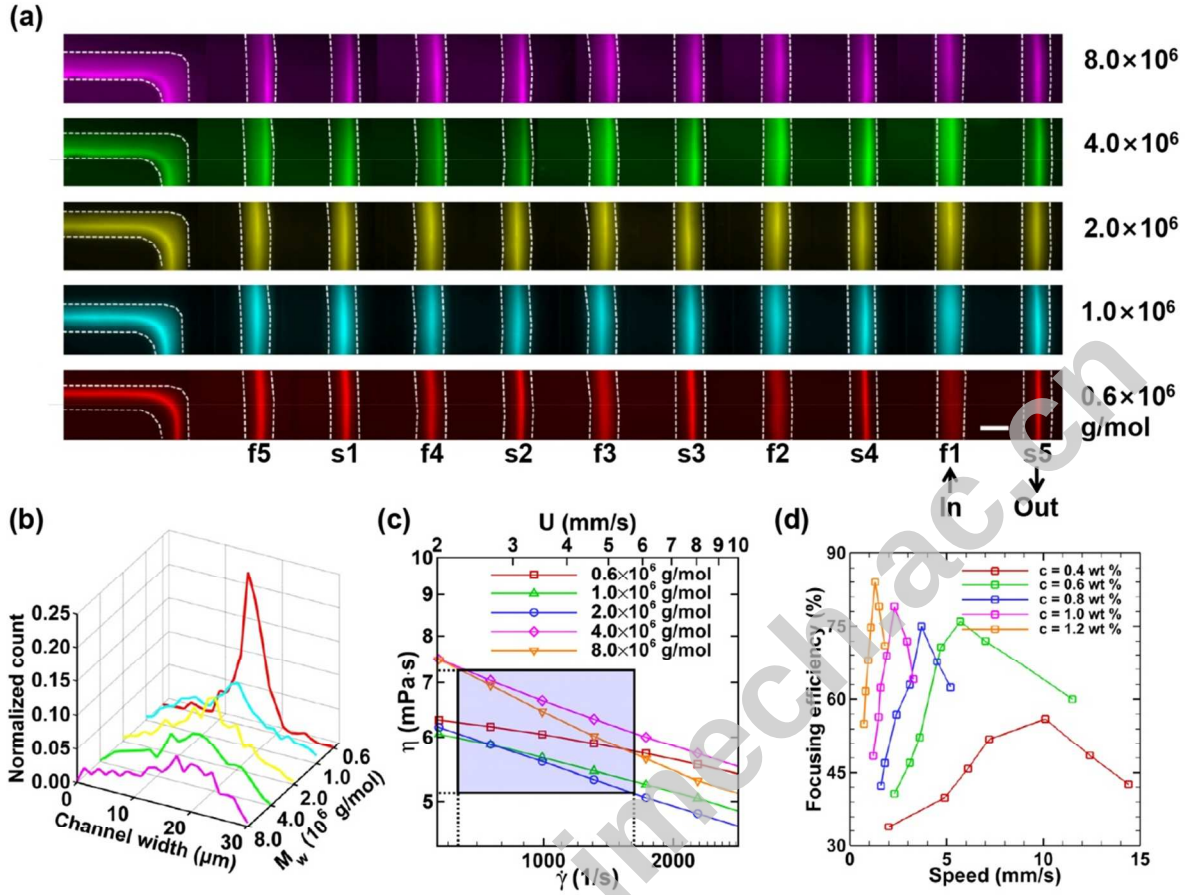

Figure 3. (a) Fluorescent trajectories of 100 nm PS particles in each loop along the double spiral microchannel with M_w ranging from 0.6×10^6 to 8.0×10^6 g/mol and (b) the particle distributions at the outlet determined by counting. (c) The measured shear viscosities of the PEO solutions with different M_w (shown in a double-logarithmic coordinate). The smallest slope shows the weakest shear thinning for M_w = 0.6×10^6 g/mol. The flow rates used for particle focusing are marked with a rectangular box. The shear viscosities and shear thinning index at a wide range of shear rates are shown in Figure S-4 in the SI†. (d) Focusing efficiencies of 100 nm particles in $M_w = 6\times10^5$ g/mol PEO solutions with c ranging from 0.4 to 1.2 wt %. Increasing c results in the increase of the maximum focusing efficiency and the decrease of corresponding optimal flow speed. The highest focusing efficiency of 84 % is achieved at c = 1.2 wt % and the flow speed of 1.3 mm/s.

polymer molecules are vulnerable to mechanical stirring). The solutions were then prepared by swinging gently for 24 – 120 hours to secure good solutions. In this work, seven different PS microspheres were used: 2000 nm, 1000 nm, 500 nm, 200 nm, 100 nm, 75 nm, and 49 nm in diameter. All fluorescent microspheres were purchased from Thermo Fisher Scientific, USA and 2000 nm ordinary ones were purchased from Wuxi Nanozymics Biotech, China. The DNA samples were prepared by diluting λ-DNA (500 μg/mL, 48.5 kbp, New England Biolabs) or DNA fragments (647 μg/mL, 15 kbp, New England Biolabs) to the same final concentration of 50 ng/mL. The concentration DNA origami samples were 200 nM. The DNA molecules and origami structures were stained with 10× SYBR Green I (Sigma-Aldrich, USA).

Experimental Procedures and Analysis. Viscoelastic solutions containing nanoparticles were injected into the microchannels using syringe pump (Pump 11 Elite, Harvard Apparatus, USA) at various constant flow rates. The fluorescent images were obtained using a fluorescent inverted microscope (Olympus IX71, Japan) equipped with an electron-multiplying charge-coupled device CCD (EMCCD, Andor DV885) and the bright-field images were obtained using an inverted microscope (Eclipse Ti, Nikon, Japan) equipped with a high-speed camera (Phantom v7.3, Vision Research Inc., USA). The fluorescent PS particles were excited by 532 nm green light, and the DNA molecules or origami structures stained by SYBR Green I were excited by 480 nm blue light. The motions of 2000 nm PS particles and platelets during the separation experiments were observed using bright-field imaging mode. The images were processed with the ImageJ software package (NIH): the time-series images (200−500 images) were stacked using z-projection with the "sum slices" and "standard deviation" options for fluorescent and bright-field images, respectively. The particle distributions were determined by manual counting for 400−500 images using ImageJ. The rheological properties of different polymer solutions were measured by a rheometer (Physica MCR301, Anton Paar GmBH, Germany) with cone−plate geometry (50 mm, 0.017 rad) at 25 °C.

RESULTS AND DISCUSSION

Focusing of 100 nm PS Particles in Different Solutions. Figure 3a shows the focusing behavior of polystyrene (PS) fluorescent particles with a = 100 nm in the aqueous solutions of PEO of five different M_w, 0.6, 1.0, 2.0, 4.0, and 8.0×10^6 g/mol. The PEO concentrations c are tuned to be 0.6, 0.4, 0.32, 0.25, and 0.2 wt %, respectively to achieve nearly identical viscosities ($6\pm2\times10^{-3}$ Pa·s) in the range of the

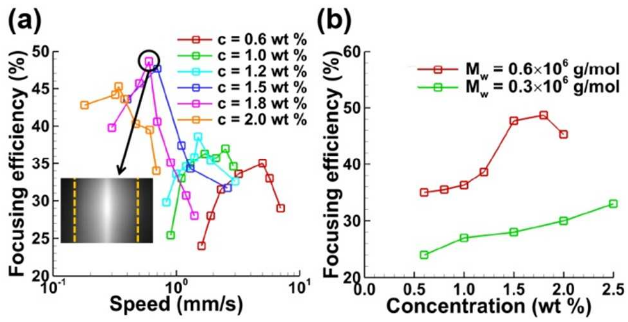

Figure 4. Focusing of 49 nm PS particles in the PEO solutions of $M_w = 0.6\times10^6$ g/mol. (a) Focusing efficiencies of 49 nm particles for c ranging from 0.6 to 2.0 wt %. The maximum of focusing efficiency reaches 49% at the optimal c of 1.8 wt %. (b) Focusing efficiencies for $M_w = 0.3\times10^6$ g/mol are much lower than those of $M_w = 0.6\times10^6$ g/mol for all the investigated c.

experimental shear rates (Figure 3c). Surprisingly, 100 nm particles are best focused with an efficiency of 76% in the solution of the lowest M_w of 0.6×10^6 g/mol (c = 0.6 wt %) at a highest channel velocity of 5.7 mm/s (1.4 μL/h). Here, we define the focusing efficiency as the fraction of particles in the central region within 1/5 channel width. In contrast, particle distribution profiles become blunt (the highest efficiency is less than 40 %) for high M_w ranging from 1.0 to 8.0×10^6 g/mol (Figure 3b), despite their longer λ (Table S-1 in the SI†). We should note that few studies used PEO of M_w lower than 1.0×10^6 g/mol, because it is a common belief that high M_w solutions of long λ favor the particle focusing.[11,17,18] Shear thinning is responsible for the insufficient focusing of 100 nm particles in PEO solutions of high M_w. Particles suspended in shear thinning viscoelastic fluids are driven away from the channel center,[19,24] due to the redistribution of elastic stress across the particle surface that in favor of wall-directed net lift force.[25] The shear thinning can be measured by the index of the power-law model for shear viscosity, which is reflected by the slope of shear-viscosity curve (Figure 3c). In the range of experimental shear rates, the solution of $M_w = 0.6\times10^6$ g/mol possesses less intensive shear thinning behavior than other higher M_w. Shear thinning can also destabilize the viscoelastic flow and trigger the onset of elastic instabilities.[26] The scaled-down channel dimension, resulting in weaker fluid inertia, further aggravates this problem because the inertia itself can stabilize elastic flows.[27] Therefore, particle focusing in such small scale is vulnerable to shear thinning.

With the optimal M_w (0.6×10^6 g/mol), we next characterize the dependence of varied c ranging from 0.4 to 1.2 wt % on the focusing of 100 nm particles (Figure 3d). The optimal focusing efficiency increases and the corresponding flow speed decreases with the increasing c. The highest focusing efficiency of 84 % is achieved at c = 1.2 wt % and the flow rate of 0.32 μL/h. We choose 0.6 wt % as the optimal c, considering the balance of focusing efficiency and throughput. To evaluate the performance of the present device, we compare our results with the previous investigation using a microtube focuser. The tube with the diameter of 5 μm enabled the focusing of 200 nm particles with the efficiency of 85% at the flow rate of 16.2 nL/h.[18] With larger channel dimension (D_h = 7.05 μm), our double spiral microchannel successfully focuses 100 nm particles at a much higher flow

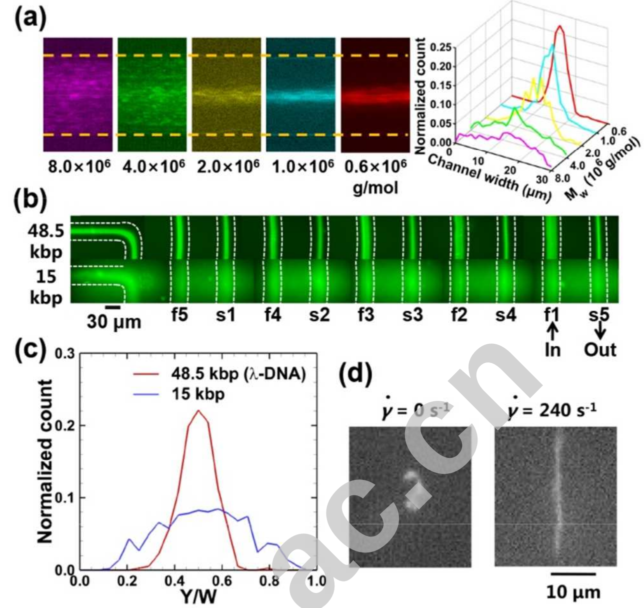

Figure 5. (a) Focusing of λ-DNA molecules (48.5 kbp) in the PEO solutions with M_w = 8.0, 4.0, 2.0, 1.0, and 0.6×10^6 g/mol and the corresponding c = 0.2, 0.25, 0.32, 0.4, and 0.6 wt %, respectively. Left: stacked images by summing 300 frames acquired at the outlet. Right: the distributions of λ-DNA molecules at the outlet determined by counting analysis. (b) Fluorescent trajectories of two types of DNA molecules (48.5 kbp and 15 kbp) in each loop along the double spiral microchannels. The concentrations of these two types of DNA are 50 ng/mL. (c) The distributions of the DNA molecules with 48.5 kbp (red) and 15 kbp (blue). (d) Conformation of the λ-DNA molecules in steady fluid (left) and sheared flow (right).

rate of 1.4 μL/h, only with slight degradation of focusing efficiency.

Focusing of Smaller PS Nanoparticles. We further extend our investigation to the regime of focusing nanoparticles with dimensions less than 100 nm. The optimal focusing efficiency of 49 nm PS particles is only 35 % in the PEO solutions with $M_w = 0.6\times10^6$ g/mol and c = 0.6 wt %, since they are much more difficult to be focused by the weak elastic forces ($F_e \propto a^3$). The increased c up to 2.0 wt % preferentially improves the focusing quality by increasing the elastic lift forces. 49 nm particles are more tightly focused at higher c (Figure 4a). The optimal focusing efficiency reaches 49% at c = 1.8 wt %, but followed by a slight decline at c = 2.0 wt %, which can be attributed to the enhanced shear thinning effect for such high c.

Rheological measurements have shown that polymer solutions with lower M_w possess wider range of c where the solutions keep weak shear thinning effects (PEO solutions used in this work possess this tendency as shown in Figure S-5 in the SI†).[28] Therefore, we investigate the possibility of better focusing of 49 nm particles in PEO solutions with M_w = 0.3×10^6 g/mol and c ranging from 0.6 to 2.5 wt % (Figure 4b). However, the focusing efficiencies for $M_w = 0.3\times10^6$ g/mol are much lower than those of $M_w = 0.6\times10^6$ g/mol for all the investigated c. The solutions with $M_w = 0.3\times10^6$ g/mol results in the weak elasticity, whose λ is over 4 times shorter than that for $M_w = 0.6\times10^6$ g/mol at the same c ($\lambda \propto M_w^{2.1}$).[29,30]

Therefore, a good carrier solution should have weak shear thinning and sufficient elasticity at the same time. In the present study, the PEO solution of $M_w = 0.6\times10^6$ g/mol is the optimal one.

Focusing of Flexible DNA Molecules. The focusing of λ-DNA molecules (48.5 kbp) is investigated for $M_w = 0.6$, 1.0, 2.0, 4.0, and 8.0×10^6 g/mol and with $c = 0.6$, 0.4, 0.32, 0.25, and 0.2 wt %, respectively. The DNA molecules are fluorescently stained by 10×SYBR Green I for observation. Like rigid PS particles, the λ-DNA molecules possess the highest focusing efficiency of 85 % for $M_w = 0.6\times10^6$ g/mol and the efficiency decreases with increasing M_w (Figure 5a), indicating that the mechanism for choosing the optimal M_w is also applied to flexible biomacromolecules. We note that, the flexibility largely disturbs the focusing of the DNA molecules and makes it more challenging for the DNAs than the rigid particles. The λ-DNA molecules, though having radii of gyration R_g of 530 nm,[31] only possess a focusing efficiency slightly higher than that of 100 nm PS particles. Smaller DNA fragments (15 kbp), with R_g of 260 nm, are focused with the focusing efficiency of 40 % (Figure 5c), much lower than that for the equal-sized 500 nm PS particles (100%, as shown in Figure 6a).

R_g generally describes the dimension of a coiled DNA molecule at equilibrium state. The flexible DNA molecules suspended in pressure-driven flows have conformation changes (Figure 5d) that affect their focusing behavior mainly in two aspects: 1) the stretching of a DNA molecule along the streamline reduces the elastic lift force on it, since the area of thrust surface and normal stress gradients stretched over by the DNA molecule both decrease; 2) the flexibility leads to additional hydrodynamic repulsion near the wall, enhancing the DNA focusing along the channel center.[32,33] The reduced focusing efficiencies of DNA molecules than rigid particles with diameters much smaller than R_g suggest that the first effect should dominate the DNA focusing.

Sheathless Separation of Synthetic and Biological Particles. The dependence of focusing efficiency on particle size and flow speed is investigated for a ranging from 49 to 2000 nm in the PEO solution with $M_w = 0.6\times10^6$ g/mol, c = 0.6 wt % (Figure 6a-b). The focusing efficiency monotonically decreases with the decreasing a: the optimal values are 100, 100, 82, 76, 55, and 33% for a = 1000, 500, 200, 100, 75, and 49 nm, respectively (Figure 6a). The optimal flow rates for various a are quite similar: 6.1±1.1 mm/s for diameters of 200, 100, 75, and 49 nm. Instead of forming clear peaks of focusing efficiency, larger particles (1000 and 500 nm) have focusing efficiencies of 100% for a wide range of flow speeds due to the strong acting elastic lift forces. In addition, particle size also affects the equilibrium position when a exceeds 1000 nm. 2000 nm particles are focused along the two sidewalls at speeds higher than 2.0 mm/s (Figure 6b). The off-center focusing stems from the enhanced compressive normal stress at the near-center side of a large particle (κ > 0.25-0.3).[19,25] We have previously reported this off-center focusing in microchannels with dimensions of ~10 μm.[19] The present finding shows that such focusing pattern still exists in a wide range of dimensions, making sheathless separation of nanoparticles from larger ones feasible.

We utilize this size-differential focusing of particles in the PEO solutions to demonstrate high-quality sorting of the

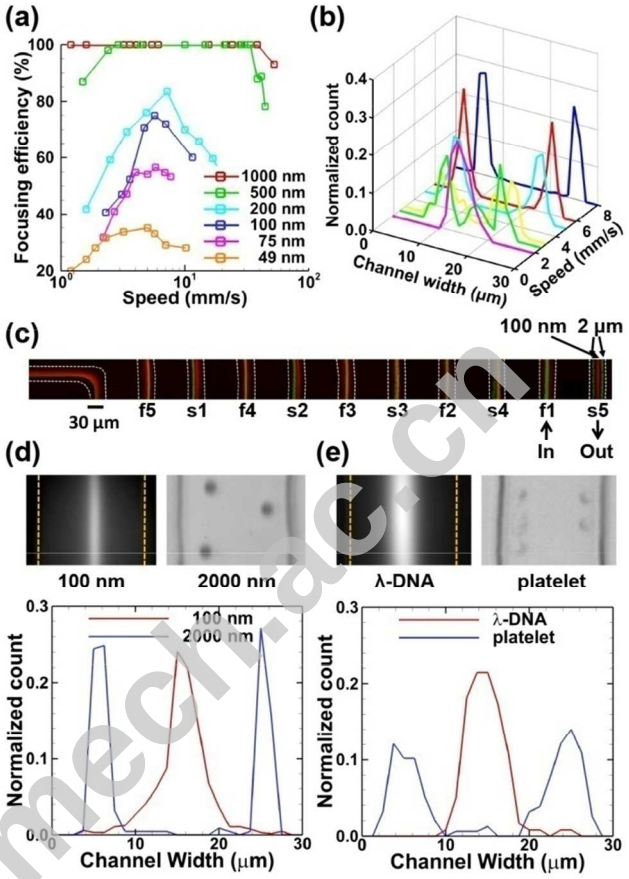

Figure 6. (a) Focusing efficiencies of PS particles with a ranging from 49 to 1000 nm for $M_w = 0.6\times10^6$ g/mol, c = 0.6 wt %. (b) The distribution profiles show that 2000 nm PS particles are focused along the sidewalls at flow speeds higher than 2 mm/s. (c-e) Size-based separation of the binary mixtures of PS particles and bioparticles at the flow speed of 5.7 mm/s. (c) The stacked image of the trajectories of 100 nm fluorescent and 2000 nm ordinary PS particles in each loop along the double spiral microchannel. The 100 and 2000 nm particles are discriminated by being marked with red and green pseudo-colours, respectively. (d) Zoom-in images of the 100 nm (stacked fluorescent image) and 2000 nm (bright-field image) particles. The counting analysis at the outlet confirms a complete separation. (e) Zoom-in images of the λ-DNA molecules (stacked fluorescent image) and platelets (bright-field image). The counting analysis at the outlet confirms a complete separation.

binary mixture with nanoparticles. We first separate the binary mixture of 100 nm fluorescent particles and 2000 nm ordinary particles and observe their focusing behaviors using fluorescent and bright-field imaging, respectively (Figure 6c-d). At the optimal flow speed of 5.7 mm/s, after passing the double spiral microchannel, the 100 nm particles are focused along the channel center whereas the 2000 nm particles are focused toward the two side walls. Figure 6d shows that in the binary mixture, the 100 nm particles are focused as tightly as they are in monodisperse dispersions, which is not disturbed by the co-existing 2000 nm particles. This should be attributed to the large separation distance (> 8μm) between the central strike of the 100 nm particles and the side strikes of the 2000 nm ones. Counting analysis quantitatively demonstrates good separation with efficiencies of 95% and 96% for the 100 and 2000 nm particles, respectively. Similarly, we successfully separate the binary mixture of the λ-DNA and the platelets in

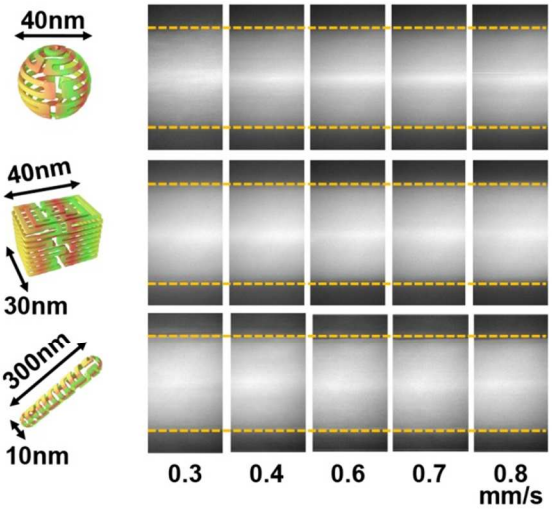

Figure 7. Focusing of three types of DNA origami structures in the PEO solution with c = 1.8 wt %. The three DNA origamis are spheres with diameters of 40 nm, short tubes with diameters of 30 nm and lengths of 40 nm, and long tubes with diameters of 10 nm and lengths of 300 nm, respectively.

PBS solution of PEO of $M_w = 0.6\times10^6$ g/mol, c = 0.6 wt % in the same channel. Platelets are biconvex discoid structures with diameters of 2-3 μm, and thus are expected to be focused along the side walls whereas the λ-DNA is tightly focused along the channel center. Figure 6e shows the size-based sorting of the λ-DNA and the platelets from their binary mixture at the outlet with the separation efficiencies of 96% and 97%, respectively. The platelets have been reported to introduce errors in real-time PCR,[34] and the present separation technique may help to improve the accuracy of DNA assessment for biological or clinical samples.

Focusing of DNA origami. We investigate the focusing of three types of DNA origami structures: spheres (40 nm in diameter), short tubes (30 nm in diameter and 40 nm in length), and long tubes (10 nm in diameter and 300 nm in length) in PEO solutions with $M_w = 0.6\times10^6$ g/mol and c = 1.8 wt % (Figure 7). All these origami structures have observable tendency of being focused along the channel center. The spherical and short-tubular origamis are focused tighter than the long-tubular ones for all flow conditions: their optimal focusing efficiencies are 33, 31, and 28%, respectively. This discrepancy is associated with the attitudes of origamis, i.e., the non-spherical origamis align their longest dimensions with the streamlines due to the compressive elastic stresses,[35] and thus the shortest dimension predominately determines the lateral lift forces. The low focusing efficiencies of the origamis are due to their small dimensions and hollowness, which lead to reduced area of thrust surface and thus make their focusing more challenging. On the other hand, the successful focusing for very small κ is valid for a wide range of channel dimensions based on our previous[19] and present observations. We believe that the origamis can be better focused in the low-viscosity viscoelastic solutions by further reducing the channel dimensions.

PVP Solutions for Nanoparticle Manipulation. We note that several previous studies have used PVP solutions with $M_w = 3.6\times10^5$ g/mol for focusing and separating microparticles.[36,37] Despite their weak shear thinning effects, the PVP solutions are not suitable for manipulating nanoparticles due to the weak elasticity and high viscosities. We investigate the focusing behaviors of 100 nm particles in 3.6×10^5 g/mol PVP solutions with c = 8 wt %, 5 wt %, and 1 wt % and a 3×10^5 g/mol PEO solution with c = 1.0 wt % (Figure S-6 in the SI†). All these PVP and PEO solutions have very weak shear thinning effects. With the same c = 1.0 wt %, the focusing efficiencies in the PVP solution are much lower than those in the PEO solution for all investigated flow speeds. With a high c = 8 wt %, the efficiencies of the PVP solution are just comparable with those of the PEO solution with c = 1.0 wt %, indicating the weak elasticity of the PVP solution. Moreover, the high viscosities of PVP solutions (~100 mPa·s for 8 wt %, a commonly used c) require extremely high driving pressure in the scaled-down channel for nanoparticle manipulation, which is difficult to achieve in conventional microfluidic devices.

CONCLUSIONS

In this work, we demonstrate the sheathless viscoelastic manipulation of a variety of nanoparticles including synthetic nanoparticles, λ-DNA molecules, and DNA origamis in a double spiral microchannel. By unconventionally using the PEO solutions of low molecular weight with minimized shear thinning, we achieve the high-quality focusing of nanoparticles down to 100 nm, outperforming the existing viscoelastic microfluidics for micro/nanoparticle manipulation (Table S-2 in the SI†). Moreover, two sets of binary mixtures, 100/2000 nm PS particles and λ-DNA molecules/blood platelets, are sorted with the separation efficiencies above 95 %. Our size-based separation technique allows for precise and relatively high throughput manipulation of the nanoscale objects in large microchannel dimensions, without resorting to the complex device design and fabrication. This versatile and label-free technique may lead to a paradigm shift in viscoelastic microfluidics for enrichment and separation of nanoparticles encountered in applications of biology, chemistry, and nanotechnology.

ASSOCIATED CONTENT

Supporting Information

Additional information, one table, and five figures as noted in the text. This information is available free of charge via the Internet at http://pubs.acs.org.

AUTHOR INFORMATION

Corresponding Author

*Phone: +86-10-82544298. Fax: +86-10-82543977. E-mail: guoqing.hu@imech.ac.cn.
*Phone: +86-10-82545621. Fax: +86-10-82545631. E-mail: sunjs@nanoctr.cn.

Notes

The authors declare no competing financial interest.

ACKNOWLEDGMENT

This work was supported financially by NSFC (11572334, 91543125, 11272321), the CAS Key Research Program of Frontier Sciences (QYZDB-SSW-JSC036), and the CAS Strategic Priority Research Program (XDB22040403) to GH and MOST (2013AA032204), NSFC (21475028, 21622503), and Youth Innovation Promotion Association CAS to JS.

REFERENCES

(1) Murphy, C. J.; Sau, T. K.; Gole, A. M.; Orendorff, C. J.; Gao, J.; Gou, L.; Hunyadi, S. E.; Li, T. *J. Phys. Chem. B* **2005**, *109*, 13857-13870.
(2) Nie, Z.; Petukhova, A.; Kumacheva, E. *Nat. Nanotechnol.* **2010**, *5*, 15-25.
(3) Hu, G.; Jiao, B.; Shi, X.; Valle, R. P.; Fan, Q.; Zuo, Y. Y. *ACS Nano* **2013**, *7*, 10525-10533.
(4) Zhang, S.; Li, J.; Lykotrafitis, G.; Bao, G.; Suresh, S. *Adv. Mater.* **2009**, *21*, 419-424.
(5) Jiang, W.; KimBetty, Y. S.; Rutka, J. T.; ChanWarren, C. W. *Nat. Nanotechnol.* **2008**, *3*, 145-150.
(6) Ai, Y.; Sanders, C. K.; Marrone, B. L. *Anal. Chem.* **2013**, *85*, 9126-9134.
(7) Han, J.; Craighead, H. G. *Science* **2000**, *288*, 1026-1029.
(8) Han, D.; Pal, S.; Nangreave, J.; Deng, Z.; Liu, Y.; Yan, H. *Science* **2011**, *332*, 342-346.
(9) Leshansky, A. M.; Bransky, A.; Korin, N.; Dinnar, U. *Phys. Rev. Lett.* **2007**, *98*, 234501.
(10) Yang, S.; Kim, J. Y.; Lee, S. J.; Lee, S. S.; Kim, J. M. *Lab Chip* **2011**, *11*, 266-273.
(11) Kang, K.; Lee, S. S.; Hyun, K.; Lee, S. J.; Kim, J. M. *Nat. Commun.* **2013**, *4*, 2567.
(12) Nam, J.; Lim, H.; Kim, D.; Jung, H.; Shin, S. *Lab Chip* **2012**, *12*, 1347-1354.
(13) Lu, X.; Xuan, X. *Anal. Chem.* **2015**, *87*, 6389-6396.
(14) Lu, X.; Zhu, L.; Hua, R.-m.; Xuan, X. *Appl. Phys. Lett.* **2015**, *107*, 264102.
(15) Lee, D. J.; Brenner, H.; Youn, J. R.; Song, Y. S. *Sci. Rep.* **2013**, *3*, 3258.
(16) Xiang, N.; Chen, K.; Dai, Q.; Jiang, D.; Sun, D.; Ni, Z. *Microfluid. Nanofluid.* **2014**, *18*, 29-39.
(17) Kim, J. Y.; Ahn, S. W.; Lee, S. S.; Kim, J. M. *Lab Chip* **2012**, *12*, 2807-2814.
(18) De Santo, I.; D'Avino, G.; Romeo, G.; Greco, F.; Netti, P. A.; Maffettone, P. L. *Phys. Rev. Applied* **2014**, *2*, 064001.
(19) Liu, C.; Xue, C.; Chen, X.; Shan, L.; Tian, Y.; Hu, G. *Anal. Chem.* **2015**, *87*, 6041-6048.
(20) Zilz, J.; Poole, R. J.; Alves, M. A.; Bartolo, D.; Levache, B.; Lindner, A. *J. Fluid Mech.* **2012**, *712*, 203-218.
(21) Xia, Y. N.; Whitesides, G. M. *Annu. Rev. Mater. Sci.* **1998**, *28*, 153-184.
(22) Wang, J.; Chen, W.; Sun, J.; Liu, C.; Yin, Q.; Zhang, L.; Xianyu, Y.; Shi, X.; Hu, G.; Jiang, X. *Lab Chip* **2014**, *14*, 1673-1677.
(23) Liu, C.; Hu, G.; Jiang, X.; Sun, J. *Lab Chip* **2015**, *15*, 1168-1177.
(24) Huang, P. Y.; Joseph, D. D. *J. Non-Newton. Fluid Mech.* **2000**, *90*, 159-185.
(25) Huang, P. Y.; Feng, J.; Hu, H. H.; Joseph, D. D. *J. Fluid Mech.* **1997**, *343*, 73-94.
(26) Wilson, H. J.; Loridan, V. *J. Non-Newton. Fluid Mech.* **2015**, *223*, 200-208.
(27) Lim, E. J.; Ober, T. J.; Edd, J. F.; Desai, S. P.; Neal, D.; Bong, K. W.; Doyle, P. S.; McKinley, G. H.; Toner, M. *Nat. Commun.* **2014**, *5*, 4120.
(28) Macosko, C. W. *Rheology: Principles, Measurements, and Applications*; Wiley-VCH: New York, 1994.
(29) Tirtaatmadja, V.; McKinley, G. H.; Cooper-White, J. J. *Phys. Fluids* **2006**, *18*, 043101.
(30) Rodd, L. E.; Scott, T. P.; Boger, D. V.; Cooper-White, J. J.; McKinley, G. H. *J. Non-Newton. Fluid Mech.* **2005**, *129*, 1-22.
(31) Bustamante, C.; Marko, J. F.; Siggia, E. D.; Smith, S. *Science* **1994**, *265*, 1599-1600.
(32) Jendrejack, R. M.; Dimalanta, E. T.; Schwartz, D. C.; Graham, M. D.; de Pablo, J. J. *Phys. Rev. Lett.* **2003**, *91*, 038102.
(33) Graham, M. D. *Annu. Rev. Fluid Mech.* **2011**, *43*, 273-298.
(34) Banas, B.; Kost, B. P.; Goebel, F. D. *Eur. J. Med. Res.* **2004**, *9*, 371-377.
(35) Huang, P. Y.; Hu, H. H.; Joseph, D. D. *J. Fluid Mech.* **1998**, *362*, 297-325.
(36) Yang, S.; Lee, S. S.; Ahn, S. W.; Kang, K.; Shim, W.; Lee, G.; Hyun, K.; Kim, J. M. *Soft Matter* **2012**, *8*, 5011-5019.
(37) Cha, S.; Kang, K.; You, J.; Im, S.; Kim, Y.; Kim, J. *Rheol. Acta* **2014**, *53*, 927-933.

For TOC only